Rock and Soil Mechanics 2026 47(8): 2638−2652 ISSN 1000−7598
https://doi.org/10.26599/RSM.2025.00370 journal homepage: rocksoilmech.whrsm.ac.cn

DOI: 10.16285/j.rsm.2025.00370 **CSTR:**32223.14.j.rsm.2025.00370

Influence of fines content on liquefaction resistance of coral sand mixtures

GU Lin-lin[1], SHI Ting-yan[1], WANG Zhen[2], MA Lin-jian[3], WANG Jian-ping[4], YE Guan-lin[5]

1. School of Safety Science and Engineering, Nanjing University of Science and Technology, Nanjing, Jiangsu 210094, China
2. School of Mechanical Engineering, Nanjing University of Science and Technology, Nanjing, Jiangsu 210094, China
3. State Key Laboratory of Explosion & Impact and Disaster Prevention & Mitigation Engineering, University of PLA, Nanjing, Jiangsu 210007, China
4. Naval Research Institute of PLA, Beijing 100170, China
5. Department of Civil Engineering, Shanghai Jiao Tong University, Shanghai 200030, China

Abstract: Coral sand (CSD) was mixed with fine soil in varying proportions within real reef ground, exhibiting intricate dynamic behaviors under cyclic loadings, such as earthquakes. Undrained cyclic triaxial tests under diverse confining pressures and cyclic loading stress ratios (CLSR) with various fines content (FC) were conducted to systematically investigate the liquefaction characteristics and excess pore water pressure (EPWP) development. The coarse-grained CSD and fine-grained CSD displayed distinct failure modes, with the fine-grained CSD exhibiting a greater propensity for liquefaction. The liquefaction resistance of CRR_{20} (cyclic resistance ratio) showed a trend of first decreasing and then increasing with the increase of FC, and reached the minimum value near the critical FC (FC_{th}). As FC and confining pressure increased, the axial deformation transformed from a gradual accumulation mode to a slow-rapid development mode. Particle breakage decreased with increase of FC but increased with confining pressure and CLSR. The plastic exhibited a trend of initial decrease followed by subsequent increase as FC rose, attaining its minimum value around FC_{th}. EPWP development curve changed from Type A to Type B as FC and confining pressure increased. EPWP exhibited differential responses during the third stage of Type B development pattern, when FC was relatively low (coarse-grained CSD), the growth rate of EPWP slowed down; while when FC was relatively high (fine-grained CSD), it continued increasing. The EPWP development of CSD mixtures exhibited notable discrepancy from that of quartz sand, thus a new unified EPWP model was proposed. The new findings obtained in this paper provided valuable insights for seismic design of infrastructure on coral island.

Keywords: coral sand; fines content; undrained cyclic triaxial test; liquefaction characteristics; particle breakage; excess pore water pressure

1 Introduction

The development and construction of coral reef projects have become a key industry focus in recent years. Coral sand (CSD), the primary material for island reefs in the South China Sea, is a special kind of marine biogenic geomaterial with low shear strength, fragility, irregular grain shape, and high void ratio, etc[1-3], different from terrigenous deposits. The application of cutter suction dredger reclamation techniques combined with dynamic compaction foundation treatment induces intergranular crushing within CSD deposits, generating fine-grained particles (particle diameter $D < 0.075$ mm). This granulometric evolution drives the formation of heterogeneous stratigraphic units exhibiting variable geo-mechanical properties[4-7]. Large scale CSD liquefaction and lateral sliding were all observed in the 1993 M_w 7.7 Guam earthquake[8], the 2006 M_w 6.7 and M_w 6.0 Hawaii Earthquakes[9], and the 2010 M_w 7.0 Haiti earthquake[10], which caused severe damage to port facilities and coastal structures. Given the frequent earthquakes and strong dynamic effects of waves in the South China Sea region, CSD areas were prone to dynamic instability phenomena such as liquefaction. Consequently, a comprehensive study on the influence of fines content (FC) on the liquefaction properties of coral sand foundations was critical for ensuring the stability and safety of offshore construction projects.

Numerous studies have examined the effects of FC on the soil dynamics. D'Appolonia et al.[11] were the first to observe its significant influence on the liquefaction susceptibility of quartz sand. Indraratna et al.[12] reported that fine particles served as lubricants at interfaces between sand grains, accelerating the development of primary volumetric strain in saturated sandy soils. Lade et al[13] reported that the FC affected the sandy soils' steady-state properties and residual strength to varying degrees. Studies had indicated that liquefaction susceptibility initially improved with greater FC before diminishing. However, the exact extent of the influence was associated with the sand

Received: 18 August 2025 Accepted: 18 November 2025
This work was supported by the National Key Research and Development Program, National Natural Science Foundation of China (52378401, 52422808) and the Fundamental Research Funds for the Central Universities (30924010840).
First author: GU Lin-lin, female, born in 1987, PhD, Associate professor, majoring in soil dynamics. E-mail: linlin_gu@njust.edu.cn
Corresponding author: WANG Zhen, male, born in 1987, PhD, Professor, research interests: mechanics of deep rock mass.
E-mail: wangzhen2012@njust.edu.cn

gradation and mineral composition of sandy soils[14-15]. Dezfulian[16] concluded that a higher FC enhanced the liquefaction susceptibility of quartz sand, whereas Shen et al.[17], Throncoso and Verdugo[18], Finn et al.[19], and Vaid[20] reached the contrasting conclusions. Cao and Law[21], Law and Ling[22], Koester[23], Singh[24] and Chien et al.[25] discovered that the liquefaction strength of quartz sand decreased before increasing with higher FC. FC was the critical factor controlling the mechanical behavior of sand[26]. When FC exceeded a critical value FC_{th}, the contact state of the sand changed from being dominated by coarse grains to being controlled by fine grains, significantly altering mechanical properties. Yang et al.[27] and Dash and Sitharam[28] found that when FC was less than FC_{th}, the reduction in the maximum shear strength decreased as FC increased. Conversely, when FC exceeded FC_{th}, the peak shear strength increased as FC increased. However, Belkhatir et al.[29] found a consistent reduction in the peak shear strength of sand-clay mixtures as FC increased. Based on previous studies, there was no consensus on how FC affected the mechanical behavior of sand. Most studies mainly concentrated on terrigenous sand, but the influence of FC on the mechanical properties of CSD had received comparatively less attention in research.

Recent studies have investigated the effect of FC on CSD properties. Hu et al. [30] discovered that the permeability of calcareous sand was primarily influenced by the FC (FC≤35%), decreasing with FC and stabilizing beyond 24%. Zhang et al. [31] and Shen et al.[32] conducted the drained triaxial tests and discovered that increasing FC could change the shear strength and strain-softening behavior of CSD. Li et al.[33] conducted ring-shear tests and observed that the strength of coral-mixed sand gradually decreased with increasing FC. The extent of particle breakage decreased with FC increasing, and the mixture containing glass beads exhibited a lower degree of breakage. Wu et al.[34] and Wu et al.[35] demonstrated that FC considerably influenced the peak dynamic shear modulus of CSD. Chen et al.[36] investigated the liquefaction susceptibility of coral soil with varying FCs (7%−42%) from the port in the eastern Pacific and proposed an excess pore water pressure (EPWP) model developed during liquefaction. Existing researches had preliminarily revealed how FC influenced the mechanical characteristics of CSD, whereas the research focusing on high FC (> 40%) levels was very limited. Researches on EPWP evolution law, particle breakage and plastic work of CSD with a quite wide range of FC during liquefaction were also very limited.

Given the frequent occurrence of seismic activity in the South China Sea and the increasing demand for infrastructure construction, exploring the liquefaction behavior of saturated CSD with wide range of FC is deadly needed. This study systematically investigates the cyclic failure process of saturated CSD mixtures with varying FC values (0%−70%) by undrained cyclic triaxial tests. Meanwhile, the influence of FC on liquefaction resistance, particle breakage, plastic work and development of the EPWP in CSD mixtures are also examined based on the particle contact state theory. The findings provided the valuable engineering guidance for the seismic design and construction of foundations built on CSD grounds.

2 Threshold fines content FC_{th}

Thevanayagam et al.[37−38] introduced the particle contact state theory to explain how FC affected the mechanical attributes of coarse-fine mixtures. By increasing the content of FC, interfacial contact states could be formed in infinite ways. Figure 1 shows that when FC was below FC_{th}, the coarse grains acted as the primary structural framework of the mixture, whereas the interstitial voids among coarse particles were filled with finer particles. The coarse grains primarily determined the mechanical behavior of the coarse and fine particle mixtures, and the mixture in the contact state of such particles was defined as coarse-grained soil[39]. When FC exceeded FC_{th}, coarse particles were suspended in fine particles, fine particles contained coarse particles, and the liquefaction behavior of the mixtures were mainly determined by the fabric of fine particles. When the contact between fine particles was destroyed, the whole sample would be destroyed, and the mixture was defined as fine-grained soil[39]. When FC was equal to FC_{th}, the coarse grains maintained direct contact. Conversely, fine grains filled the voids between them, and the seismic behavior of the mixture transited from coarse-grained soil to fine-grained soil, which was defined as in-transition soil[39]. It could be seen that FC_{th} represented a critical parameter for differentiating the various contact states within coarse-fine mixtures.

The theoretical method for determining the coarse and fine particle mixture FC_{th} was based on a binary packing model. The idealized binary packing model had three fundamental assumptions[39]: i) it consisted of only two distinct types of coarse and fine particles; ii) the ratio of coarse to fine particle sizes was large; and iii) the coarse particle contact was unaffected by fine particles, and vice versa. The void ratio e of the soil mixtures satisfying the binary packing model was shown in Fig.1. The value of e for mixtures with different FCs was determined by FC and the coarse particles void ratio e_c, fine particles void ratio e_f, specific gravity of coarse particle G_c, and the specific

gravity of the fine particles G_f. When FC< FC_{th}, the theoretical formula for calculating the e of the coarse-grained mixture shown in section AB of the Fig.1 was defined as

$$e=(1+e_c)/\left(1+\frac{n_f G_c}{n_c G_f}\right)-1 \tag{1}$$

When FC>FC_{th}, the theoretical formula for calculating the e of the fine-grained mixture shown in section BC was defined as

$$e=e_f/\left(1+\frac{n_c G_f}{n_f G_c}\right) \tag{2}$$

Therefore, the FC_{th} for distinguishing coarse-grained soil from fine-grained soil was the FC of the mixture corresponding to point B in Fig.1. The FC_{th} of the coarse and fine particle mixtures could be calculated by combining equations (1) and (2), and its expression was as follows:

$$FC_{th}=\frac{e_c}{e_f n+e_c+n} \tag{3}$$

where $n=G_c/G_f$. Since the specific gravity of calcareous sandy soil was generally around 2.7 to 2.8, n was usually taken as 1.0. Thus, the above formula could be simplified as

$$FC_{th}=\frac{e_c}{e_f+e_c+1} \tag{4}$$

As e of the mixture was in the range, a specific mixture did not exhibit a single FC_{th}. When a mixture was within this transitional range, it was referred to as an intermediate-state soil. The mechanical attributes of the mixture were influenced by the fine and coarse-grained structures [40].

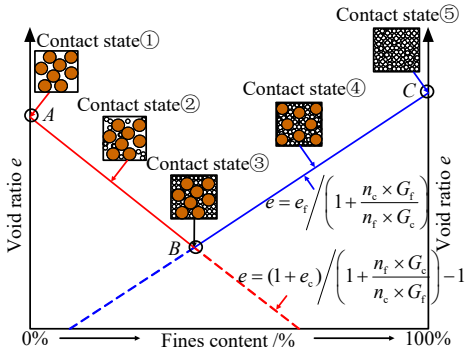


Fig. 1 Binary packing model[40]

3 Test materials and methods

3.1 Materials

The CSD used in this study was collected from a reclaimed island reef in the South China Sea. It exhibited a white hue, lacked cohesiveness, featured a rough surface texture, demonstrated low single-particle strength, and possessed a brittle consistency. After the samples were dried and cooled to room temperature, they were sieved according to the *Standard for geotechnical test methods* (GB/T 50123−2019)[41]. Sieving was conducted through a 0.075 mm sieve, with the coral sand with a particle size less than 0.075 mm sieve regarded as fine particles, and coral sand particles ranging from 0.075 to 3 mm classified as coarse particles.. Samples with different FCs were prepared by mixing coarse and fine particles in varying proportions.The coarse CSD particles exhibited void ratios ranging between 1.16 and 1.54, whereas the fine CSD grains ranged from 0.70 to 1.80, representing the wider variability of conditions in practical hydraulic filling projects. According to Equation (4), the calculated FC_{th} values ranged from 35% to 40.5%. Therefore, when FC<35%, the mixture was classified as coarse-grained CSD; when FC>40.5%, the mixture was classified as fine- grained CSD; when FC was between 35% and 40.5%, the mixture was in-transition CSD. Specimens with FC of 0%, 10%, 30%, 50%, and 70% were carefully prepared to investigate the influence of FC on the liquefaction characteristics of CSD mixtures. Table 1 illustrates the fundamental index properties characterizing CSD mixtures across varying FC levels. The skeleton pore ratio e_k is the ratio of particle pore volume to particle volume in the mixture, used to describe the contact state of the skeleton particles constituting the coarse-fine particle mixture[42].. Figures 2 and 3 illustrate the particle distribution curves and maximum and minimum void ratios. Figure 3 depicts the maximum and minimum void ratios decreased before increasing, reaching the minimum value near FC_{th}.

Table 1 Physical properties of CSD mixtures

Fines content /%	Mean grain size d_{50} /mm	Maximum dry density ρ_{dmax} /(g·cm^{-3})	Minimum dry density ρ_{dmin} /(g·cm^{-3})	Void ratio e	Skeleton void ratio e_k
0	2.330	1.27	1.08	1.24	1.24
10	2.210	1.50	1.23	1.06	1.29
30	2.010	1.69	1.28	0.69	1.41
50	0.082	1.77	1.25	0.67	1.34
70	0.045	1.71	1.16	0.82	1.17
100	0.026	1.65	1.00	0.92	0.92

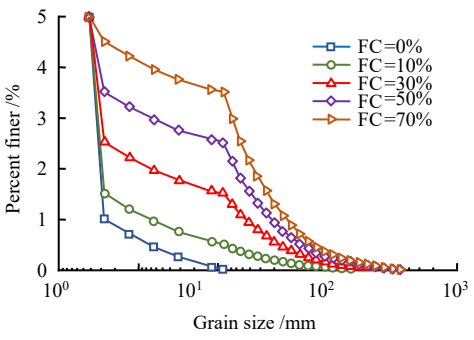


Fig. 2 Particle size distribution curves

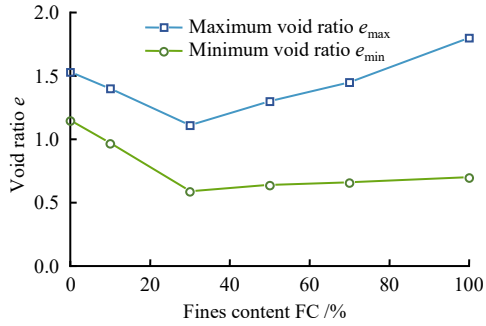


Fig. 3 Variations of e_{max} and e_{min} of CSD mixtures with FC

3.2 Methodology

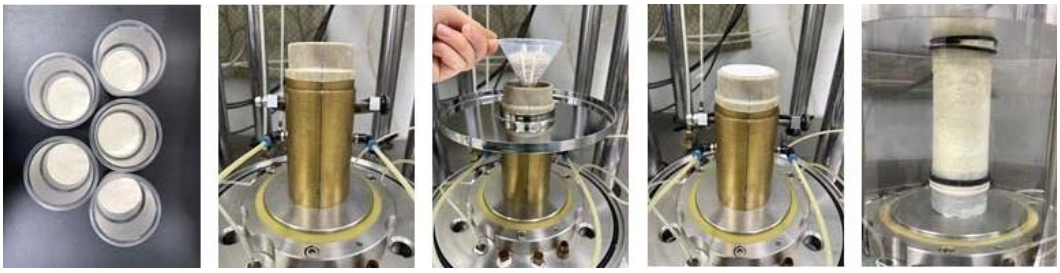
The experiment employed a SJTU-HAC shear triaxial apparatus. The test apparatus consists of five main parts: a torque servo circuit control system, a triaxial confining pressure chamber, a volumetric deformation measurement system, a data acquisition system, and an automatic pneumatic feedback regulation system. The axial stress sensor transducer had a 3 kN capacity with a minimum accuracy of 0.3 N. The displacement transducer offered a range of 20 mm with a minimum precision of 0.003 mm, the pore pressure sensor offered the 1 MPa range, and its minimum accuracy reached 0.1 kPa.

Considering the limited thickness of the constructed layer of island reefs, the number of structures built on island reefs was low. Therefore, additional stress applied to a foundation composed of CSD was typically limited. Effective confining pressures of 100, 300, and 500 kPa were employed to enhance the practical relevance of this study. Isotropic consolidation was applied to all samples, and three cyclic stress ratios (CLSR= $\sigma_d / 2\sigma'_{3c}$) were considered for each confining pressure. σ_d is cyclic loading stress ratio. Because the CSD on which island reef foundations were constructed was usually quite dense, specimens with a relative density of 80% were used for the cyclic undrained triaxial tests. The specific testing plans are presented in Table 2.

Table 2 Undrained cyclic triaxial shear test scheme for coral sand mixtures

Fines content /%	Effective confining pressure σ'_{3c} /kPa	Cyclic loading stress ratio	Relative density D_r /%
0	100	0.30, 0.35, 0.40	
0	300	0.20, 0.25, 0.30	
0	500	0.15, 0.20, 0.25	
10	100	0.30, 0.35, 0.40	
10	300	0.20, 0.25, 0.30	
10	500	0.15, 0.20, 0.25	
30	100	0.20, 0.30, 0.40	
30	300	0.20, 0.25, 0.30	80
30	500	0.15, 0.20, 0.25	
50	100	0.15, 0.20, 0.30	
50	300	0.15, 0.25, 0.30	
50	500	0.15, 0.20, 0.25	
70	100	0.15, 0.20, 0.25	
70	300	0.20, 0.25, 0.30	
70	500	0.15, 0.20, 0.25	

Figure 4 illustrates the preparation process of CSD specimens. The cylindrical specimens were Φ50 mm × 100 mm (diameter× height). The relative density D_r was controlled using the dry deposition method to ensure the uniformity of the samples. The masses of the coarse and fine grains required for each layer of the mixed specimens were accurately weighed and thoroughly mixed before being carefully poured into a rubber membrane in five equal portions. Before depositing the subsequent layer, the surface of each underlying layer was carefully roughened to minimize the occurrence of discontinuities within the sample. During the sample saturation process, carbon dioxide was injected into the sample for no less than 1 hour to promote saturation, which was followed by head saturation for 3 to 4 hours or more. Finally, the staged back-pressure saturation was implemented to ensure that the *B*-value of the sample was not lower than 0.95.



(a) Sample preparation (b) Membrane attachment (c) Sample filling (d) Preparation completion (e) Back pressure saturation

Fig. 4 Sample preparation process for CSD mixture

After saturation was completed, the sample was subjected to isotropic consolidation, and the duration of each consolidation stage was no less than 1 hour. Subsequently, the specimen was uniformly consolidated to the specific effective confining pressure, and the cyclic load of 0.1 Hz was applied.

3.3 Criteria for failure of CSD mixtures

Various factors, including the particle shape, skeleton structure, and soil materials, influence the determination of the destruction criterion. Selecting a suitable failure criterion for CSD mixtures is crucial for investigating their undrained liquefaction resistances.

Figures 5 and 6 illustrate the representative outcomes of the cyclic undrained triaxial tests for coarse-grained CSD (FC= 0%) and fine-grained CSD (FC=70%), respectively. Notably, the evolution curves of the excess pore water pressure (EPWP) ratio (R_u-N), axial strain (ε_a-N), and the stress-strain relationships exhibit significant disparities between these two types of sand, leading to distinct cyclic failure mechanisms.

Figure 5 depicts the typical experimental results for the coarse-grained CSD. As the cyclic numbers N increased, the voids within the skeleton of the coarse particles progressively diminished, leading to a progressive increase in EPWP and a decrease in the effective stress. When the double amplitude axial strain ε_{DA} attained 3.1%, R_u reached its maximum value and subsequently stabilized at a level below 1. The strong chain of "coarse grain-coarse grain" played a dominant role, and the soil sample still exhibited a comparatively substantial residual strength. As the continued cyclic loading persisted, the contacts among the skeletal particles were disrupted, leading to their slippage and rearrangement. This process resulted in the formation of new contact states, which were subsequently destroyed once again. The soil skeleton thus entered a cyclic process characterized by "destruction, reorganization, and subsequent re-destruction". During this process, there was no increase in EPWP; however, the cumulative plastic strain ε_p generated by the specimen escalated with the number of loading cycles N and ultimately surpassed 5%, and culminating in specimen failure. This failure mode results from the progressive accumulation of deformation, and such a failure phenomenon was termed cyclic flow. Adopting 5% as the criterion for the failure of coarse-grained CSD aligns with the research findings of Wu et al. [43].

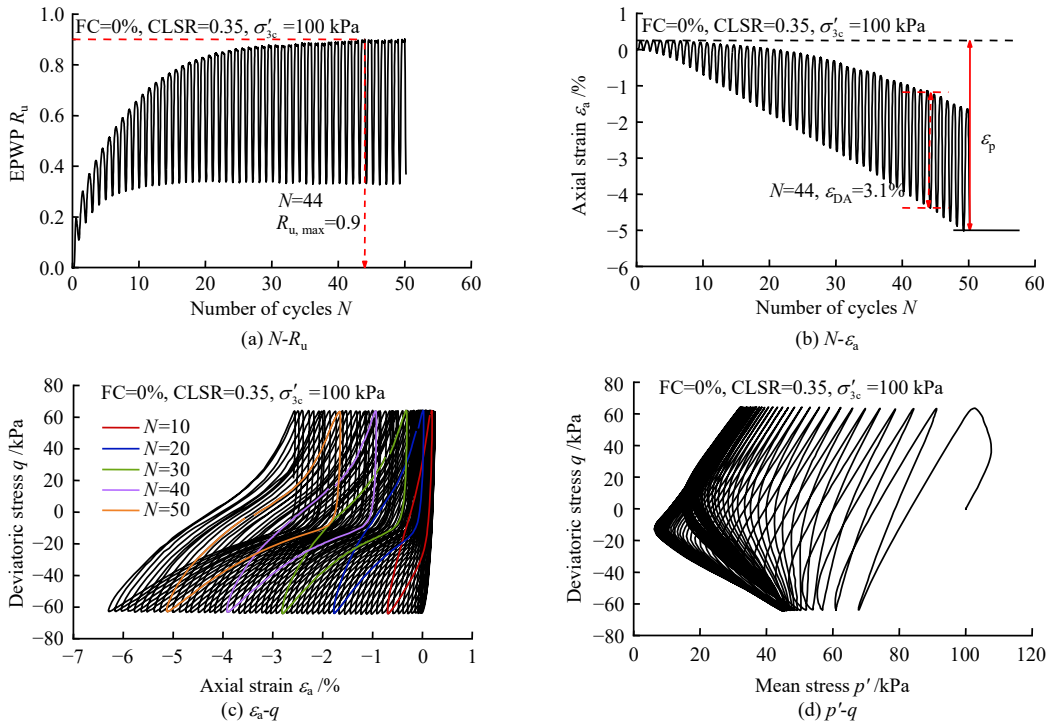


Fig. 5 Results of typical cyclic undrained triaxial test on coarse-grained CSD

Figure 6 shows representative test results for the fine-grained CSD. EPWP accumulated rapidly during the initial cyclic loading. When R_u=1, the double amplitude axial strain ε_{DA} developed sharply and exceeded 5%, and the sample reached the initial liquefaction.. For fine-grained CSD, the skeletal structure transitions to a state dominated by fine particles, wherein certain robust sand-sand force chains are substituted by weaker sand-fine particle and fine particle-fine particle force chains. Under the cyclic loading, all contacts among the fine particles constituting the soil skeleton are disrupted, resulting in all soil particles entering a suspended state and experiencing a complete loss of shear strength. Consequently, it became challenging for the soil skeleton particles to reassemble, causing the entire soil specimen to exhibit fluid-like behavior. Cyclic loading did not induce an increase in the ε_p of the sample, whereas ε_{DA} rapidly escalates within a relatively short timeframe. This phenomenon was called "cyclic liquefaction". The failure criterion of fine-grained CSD was "ε_{DA}=5%", consistent of the research findings of Wu et al.[43].

It was found that fine-grained CSD was more likely to liquefy than coarse-grained CSD. Therefore, during the dynamic compaction reinforcement process of the foundation, the generation of fine particle content should be minimized as much as possible.

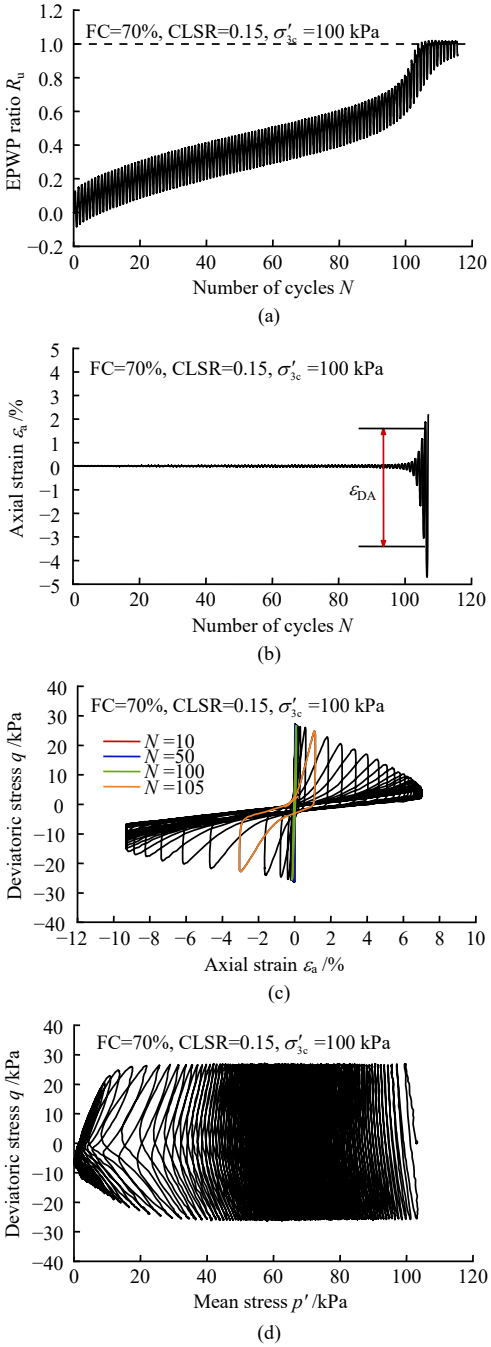


Fig. 6 Results of cyclic undrained triaxial test results on fine-grained CSD

4 Test results and discussion

4.1 Influence of FC on liquefaction resistance of CSD mixtures

The liquefaction resistance was an essential index for characterizing soil liquefaction. The correlation between CLSR and N_f was considered the liquefaction resistance (where N_f signified the number of cycles specified when the sample reached the specified failure criterion). As shown in Fig.7, N_f and CLSR were approximately in an exponential relationship under a specific confining pressure, and N_f increased as CLSR decreased. The CLSR required for the mixture to satisfy the cyclic failure criterion ranged from 0.15 to 0.4.

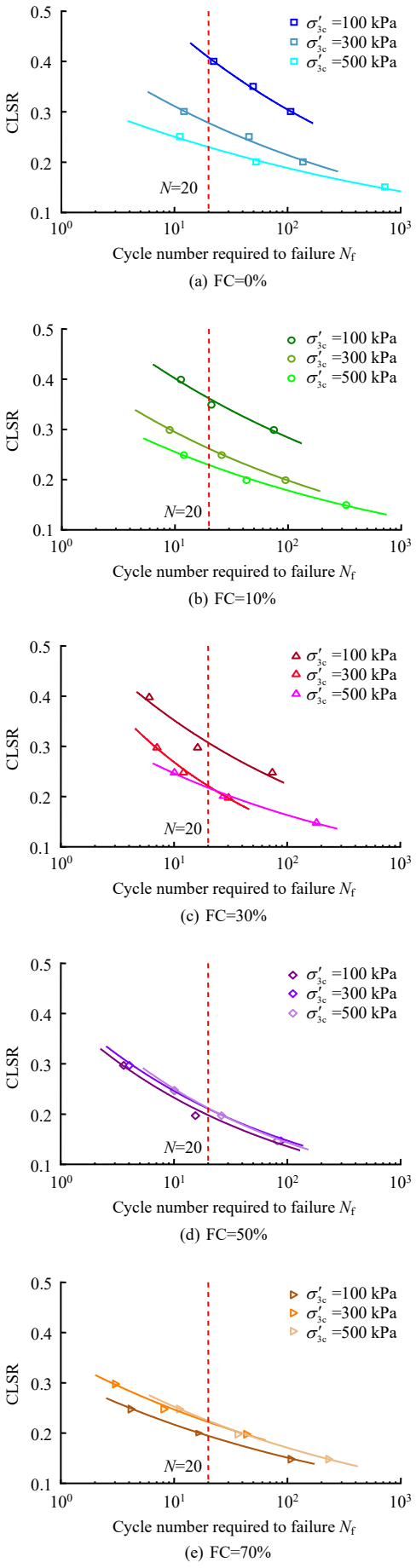


Fig. 7 Liquefaction resistances of CSD mixtures with different FCs

For the coarse-grained CSD, the liquefaction resistance curve shifted downward with increasing confining pressure, that is, the liquefaction resistance gradually decreased. Under a small confining pressure (100 kPa), CSD particles were not prone to breakage, and the stable skeletal structure could effectively resist shear deformation. The EPWP accumulated slowly, and the effective stress path slowly shifted to the left. As the confining pressure increased, it not only inhibited the shear dilatancy but also intensified the particle breakage, which reduced the strength of the soil skeleton. This led to a rapid rise in EPWP, causing the effective stress path to rapidly shift to the left and the N required to reach liquefaction failure decreased, ultimately resulting in a significant decrease in the liquefaction resistance.

Conversely, the fine-grained CSD exhibited low permeability and poor structural stability. Under a smaller confining pressure, its fragile skeletal structure rapidly destabilized under shearing, causing a sharp increase in EPWP, which led to a rapid left shift of the effective stress path and quickly reached the fluid liquefaction state. With increasing confining pressure, the particles were arranged more closely, the inter-particle contact force increased, and the soil skeleton could withstand larger external loads. The development of the effective stress path slowed down, and the N required to reach liquefaction failure increased, thereby enhancing the liquefaction resistance.

The cyclic resistance ratio (CRR) of soil was defined as the CLSR required for sandy soil to achieve cyclic failure under a specific cyclic loading number N[44]. For a magnitude 7.5 earthquake, the CLSR corresponding to the N_f=20 proposed by Martin et al.[45] was adopted as the CRR of the CSD mixture, denoted as CRR_{20}, as depicted by the red dotted line in Fig.7. To analyze the cyclic resistance of sand with varying FCs, CRR_{20} was normalized. As illustrated in Fig.8, the normalized CRR_{20} of CSD mixtures initially decreased before increasing with an increased FC. FC_{th} corresponded to the minimum CRR_{20} predicted by the binary packing model was within a range of 35%-40.5%, which was consistent with the results of Polito and Martin[14], Koester[23], Wu et al.[43], and Karim and Alam[46]. This indicated that the liquefaction resistance initially declined before subsequently increasing with increasing FC, reaching a minimum value at FC_{th}. However, variations in the fundamental physical properties of the mixtures led to different CRR_{20} for various FC mixtures. Therefore, in engineering practice, the CSD in the vicinity of FC_{th} should be avoided when choosing hydraulic reclamation materials.

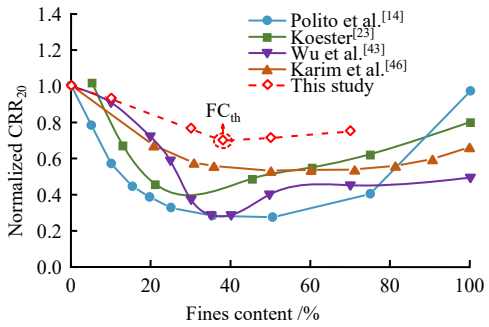


Fig. 8 Correlation between liquefaction resistance and FC

4.2 Influence of FC on deformation of CSD mixtures

The evolution of the strain in soil samples could reflect, to some extent, the development of liquefaction under undrained cyclic shear conditions. Fig.9 illustrates the development curves of the strain with N for CSD mixtures with distinct FCs under various confining pressures and CLSRs. As the CLSR increased, the N required for specimen deformation and failure decreased, and the position of instability appeared at a higher strain level. This phenomenon could be explained by the susceptibility of CSD particles to breakage during cyclic loading. Specifically, the specimens failed more rapidly under high CLSR conditions, significantly shortening the time required for particle rearrangement and adjustment. EPWP continuously accumulated and increased during this process, leading to a higher accumulation of strain.

When FC and confining pressure conditions were low (FC=0%-10%, σ'_{3c} = 100 kPa), the specimen exhibited limited deformation during each cyclic loading. This deformation gradually accumulated with increasing N, and the specimen reached the failure criterion after multiple shearing cycles. Nevertheless, as FC and confining pressure increased, the strain development pattern of CSD mixtures changed significantly from a gradual accumulation development pattern to a slow-rapid development pattern. At the initial cyclic loading, the deformation was nearly undeveloped; while, as N increased, the strain developed rapidly when it reached the critical point, leading to rapid liquefaction failure.

4.3 Influence of FC on particle breakage of CSD mixtures

The particle breakage characteristics were investigated through a particle-size sieving test on CSD mixtures before and after undrained cyclic triaxial tests. To ensure measurement accuracy, all specimens were oven-dried at 50°C until a constant weight (mass variation $\leqslant$ 0.1%). After cooling, each specimen was sieved three times, and the average value was adopted. This method prevented segregation by eliminating fine-particle agglomeration and moisture interference, thereby ensuring reliable gradation measurements. The relative breakage proposed by Hardin[47] was employed to quantify the amount of particle breakage. In this

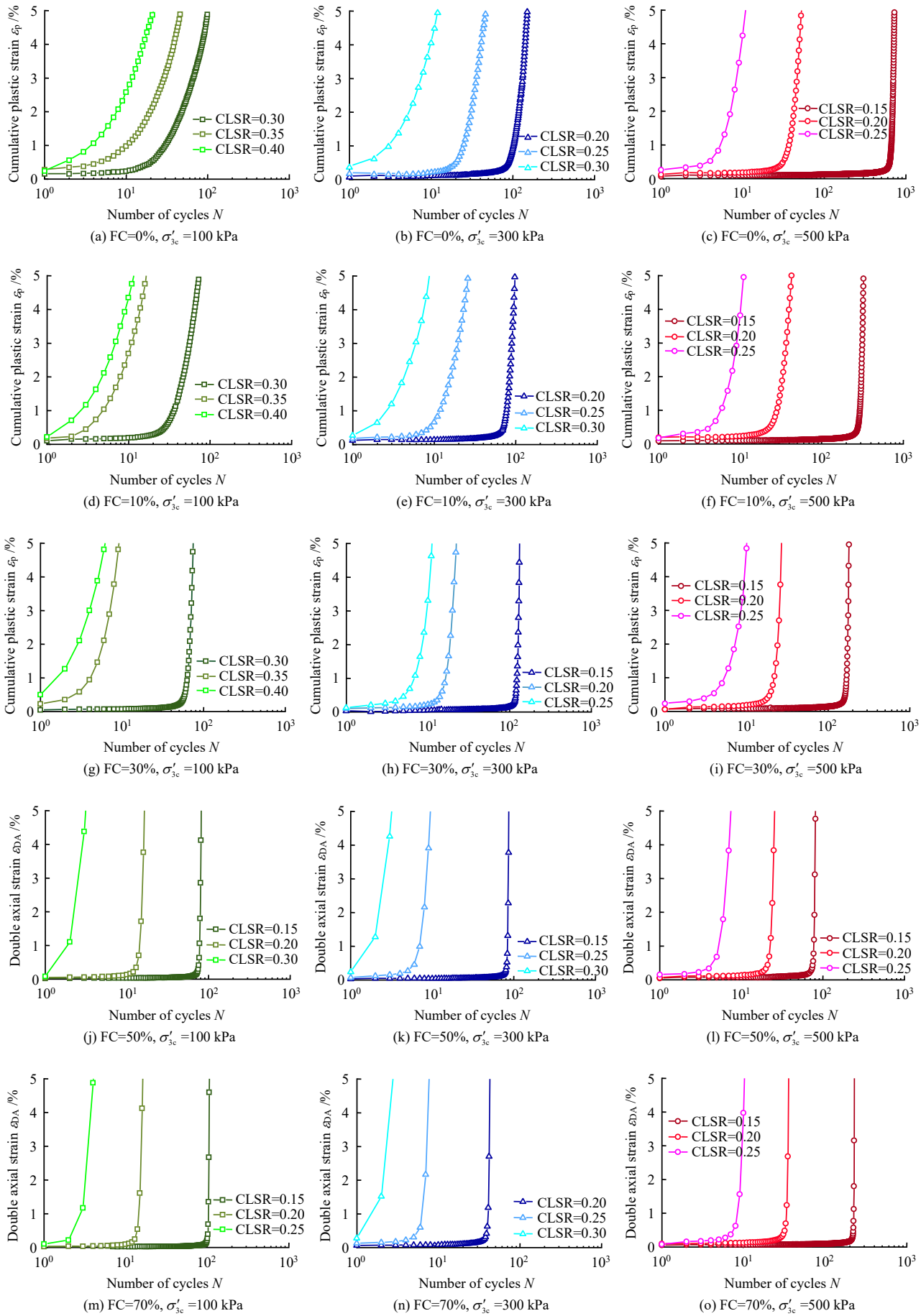


Fig. 9 Strain development curves of CSD mixtures with different FCs

model, the area enclosed by the particle size distribution curve and the vertical line D=0.074 mm was referred to as the initial crushing potential B_{P0}, based on the assumption that particles smaller than 0.074 mm would not undergo further crushing. After the sample was subjected to loading and crushing, the area enclosed by the post-crushing particle size distribution curve, the initial curve, and the vertical line D=0.074 mm was defined as the total breakage B_t. The relative breakage B_r was denoted as

$$B_r = \frac{B_t}{B_{p0}} \tag{5}$$

As shown in Fig.10, when FC=0%, due to the high proportion of coarse particles and numerous internal voids, the sample was more likely to particle breakage under cyclic loading, resulting in the most significant change in the gradation curve. As the FC increased to FC=10%, the degree of particle breakage decreased remarkably, and the variation range of the gradation curve reduced, indicating that the filling effect of fine particles increased the contact area between particles and reduced particle breakage. When the FC exceeded 30%, the particle breakage rate was less than 1%, which could be ignored.

Since the gradation curve differences under FC ⩾ 30% were no longer obvious, Fig.11 was used to analyze the effects of confining pressure and CLSR on particle breakage. As illustrated in Fig.11, the particle breakage rate increased with increasing confining pressure. This was because high confining pressure elevated the contact stress between particles, making the contact points or contact surfaces more prone to generating high local stress, thus leading to particle breakage. Simultaneously, the increase in CLSR exacerbated dislocation and back-and-forth friction between particles, further intensifying particle breakage.

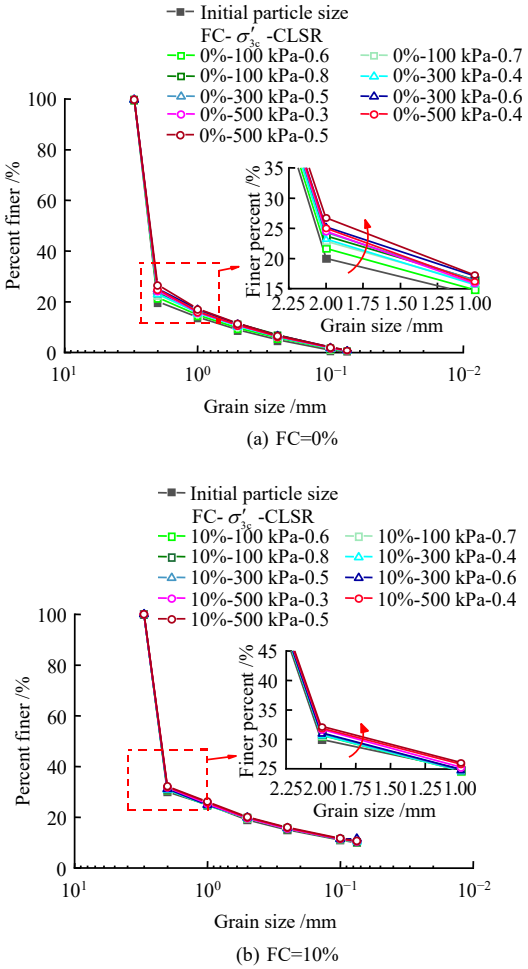


Fig. 10 Particle size distribution curves after triaxial shearing with different FCs

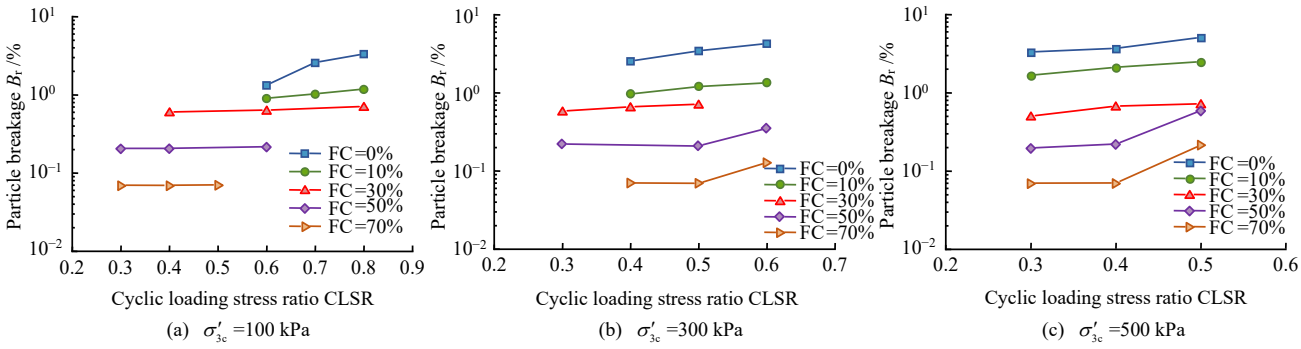


Fig. 11 Particle breakage of CSD mixtures with different FCs

4.4 Influence of FC on plastic work of CSD mixtures

The FC was an essential factor that influenced the liquefaction properties of CSD mixtures. This study investigated how FC influenced plastic deformation by analyzing the variation in plastic work W_p in CSD mixtures with different FC values. The work expended per unit volume of soil under triaxial loading conditions during a strain increment was calculated using the following equation[48]:

$$\delta W = p'\delta\varepsilon_v^p + q'\delta\varepsilon_s^p \tag{6}$$

where W represented the energy (or work) performed on the soil element of unit volume, q' signified the deviatoric stress, ε_s^p signified the plastic shear strain,

p' represented the mean effective stress, and ε_v^p signified the plastic volumetric strain. There was no volumetric strain due to the undrained triaxial test, and equation (7) can be directly used for the calculation:

$$\delta W = q'\delta\varepsilon_s \quad (7)$$

The plastic work was primarily dissipated during shearing through particle friction, rearrangement, and particle breakage. Fig.12 shows that the plastic work of CSD mixtures initially decreased before increasing with an increase in FC. For coarse-grained CSD, the rise in FC not only effectively inhibited the particle breakage rate of the mixtures, thereby reducing the energy consumed by particle breakage, but also decreased the liquefaction resistance, leading to specimen failure and a consequent decrease in plastic work. When FC approached FC_{th}, the plastic work reached its minimum value. At this FC level, the interparticle contacts had not yet formed a stable force chain structure, resulting in the lowest liquefaction resistance and higher susceptibility to failure under cyclic loading. As the FC further increased, the soil translated into fine-grained CSD, its liquefaction resistance gradually increased, and the interparticle contacts shifted toward surface contact. When the soil underwent "cyclic liquefaction" under cyclic loading, more energy was required to overcome the frictional resistance, increasing the plastic work.

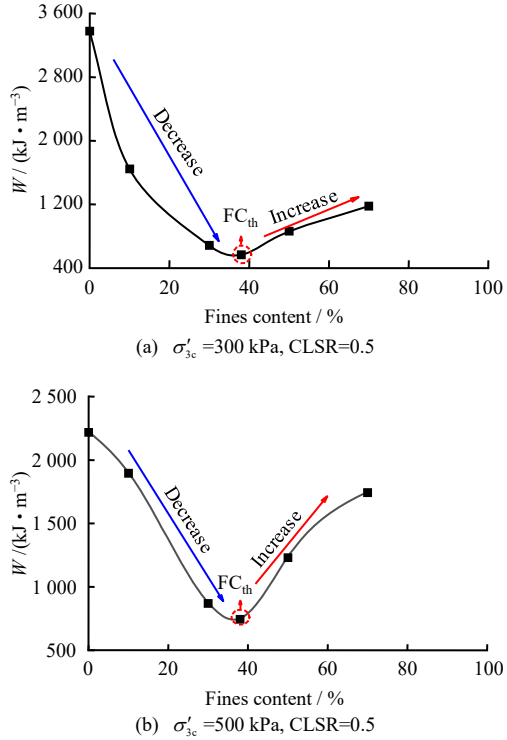


Fig. 12 Plastic work development in CSD mixtures with different FCs

4.5 Development of EPWP

The continuous accumulation of EPWP was a significant factor for the failure of CSD mixtures under the cyclic loading. Zhang and Xie[49] classified EPWP development curves under cyclic loading with constant stress amplitude into three types: Types A, B, and C, as shown in Fig.13. Type A curves were typically observed in the clayey silt, exhibiting a rapid-stable development pattern characterized by an initial rapid increase in EPWP, followed by a gradual slowing of the growth rate, which eventually stabilized and led to sample failure. Type B curves were commonly associated with the liquefaction process of sand, showing a rapid-stable-fast S-shaped growth pattern. Type C curves were predominantly observed for the light clay. The soil density, consolidation stress ratio, and CLSR influenced distinct EPWP growth patterns. The CSD mixtures used in this experiment was the sand-silt mixture, and its pore structure was significantly different from that of light clay. Consequently, EPWP development pattern of Type C was not observed.

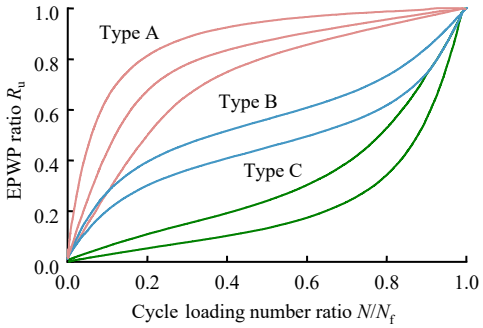


Fig. 13 Excess pore water pressure growth pattern

Fig.14 illustrates the development curves of R_u with the cyclic loading number ratio N/N_L of CSD mixtures under varying confining pressures and CLSR conditions. For coarse-grained CSD, when FC=0%-10% and σ'_{3c} = 100 kPa, EPWP development curves exhibited typical Type A characteristics and a higher CLSR resulted in a rapid increase in the growth rate of EPWP. When CLSR was constant, the EPWP development curve gradually changed to a Type B growth pattern as FC and confining pressure increased. For fine-grained CSD, the curves tended to be concentrated under different confining pressures and CLSR conditions as FC increased. When FC=70%, the influence of FC on EPWP substantially exceeded the confining stress and CLSR, and the R_u development curves all showed the Type B growth pattern.

In this paper, the A-type EPWP development curve did not exist in all CSD mixtures with different FCs. Therefore, it only focused on the evolution law governing the B-type EPWP development curve, in order to investigate how FC affected EPWP development of CSD mixtures. Fig.15 shows the typical EPWP development patterns of Type B for both coarse-

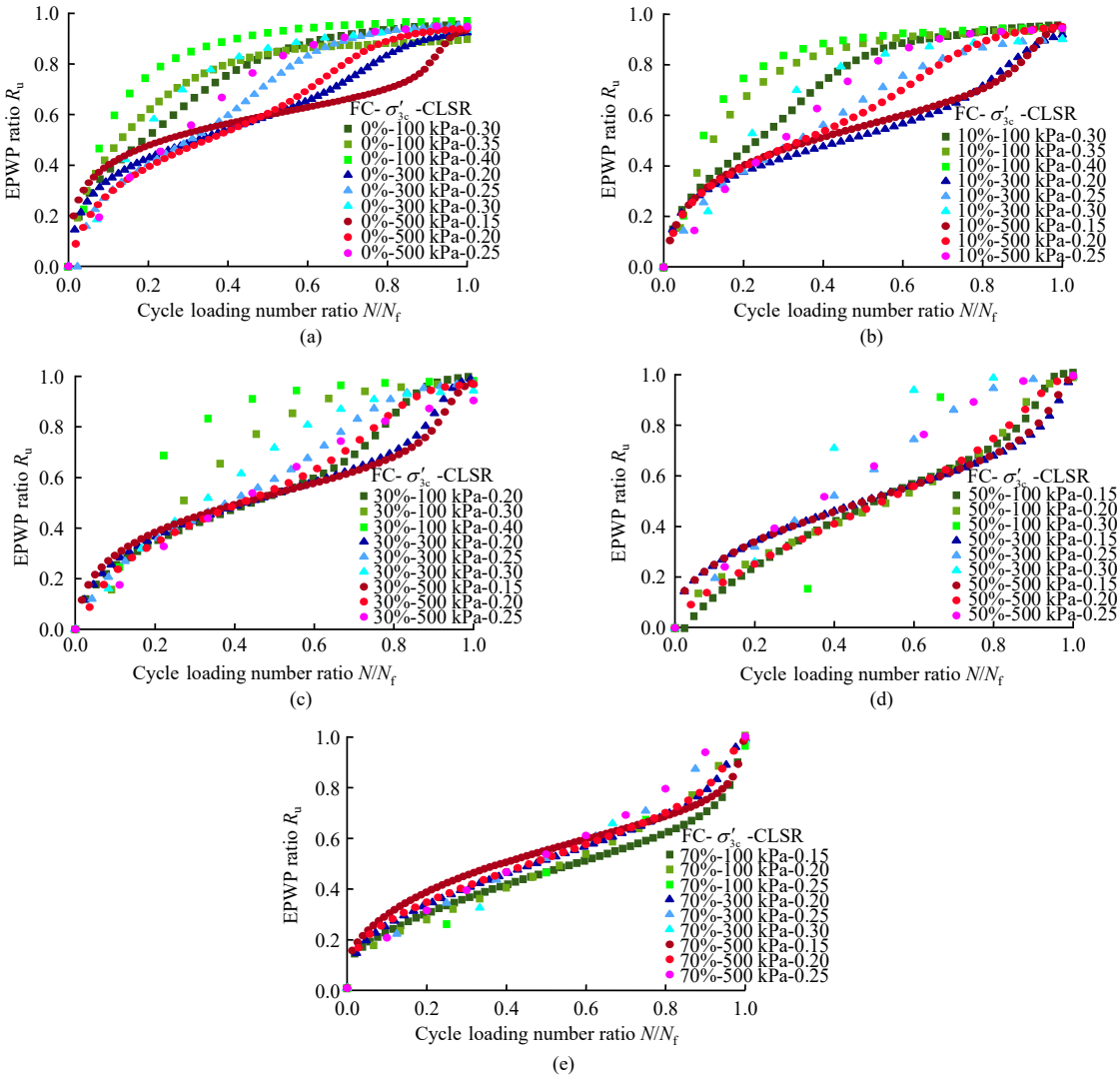


Fig. 14 Excess pore water pressure development in CSD mixtures with different FCs

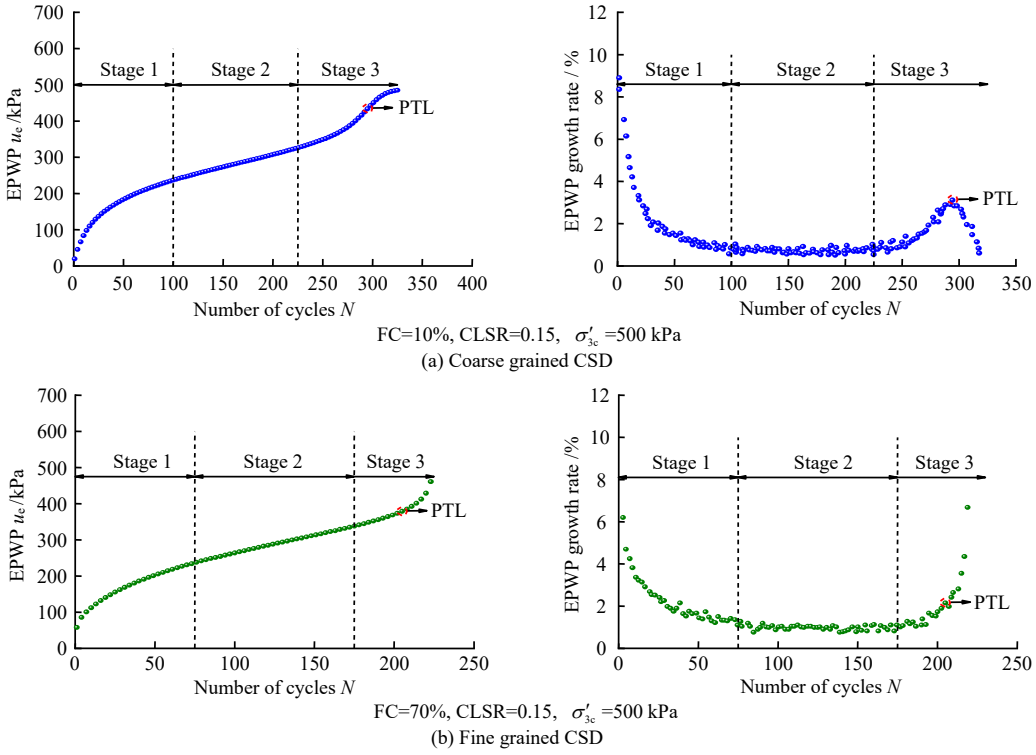


Fig. 15 Typical excess pore water pressure development pattern in CSD

grained and fine-grained CSD, exhibiting three distinct stages in the S-shaped growth pattern.

(1) Initial stage. Because the pore volume was constant under undrained triaxial tests, the shear contraction of the soil skeleton resulted in a rapid increase in EPWP under cyclic loading.

(2) Stable development stage. As the cyclic loading continued, the particles continued to rearrange, EPWP increased slowly, and the rate of development tended toward stability, and the growth trends of the coarse-grained and fine-grained CSD were similar in the first two stages.

(3) Rapid development stage. EPWP growth of coarse-grained and fine-grained CSD presented different responses after the cyclic stress path crossed the phase transformation line (PTL). The coarse-grained CSD entered a state of "cyclic flow", and EPWP continued to accumulate with the EPWP growth rate decreasing. However, near the PTL, the fine-grained CSD entered the state of "cyclic liquefaction." At this moment, the effective stress borne by the soil grains was completely transformed into EPWP, leading to a rapid increase in EPWP with a rapid growth rate.

4.6 Prediction model for EPWP

Lee and Albaisa[50] obtained the maximum and minimum boundary of the EPWP development curve for Monterey sand through numerous experiments, as shown by the shaded line in Fig.16. These findings indicated that the limitations of Monterey sand did not apply to CSD. The generation range of EPWP of CSD mixtures surpassed the upper limit of Monterey, which showed that CSD exhibited a quicker cumulative rate of EPWP and a more significant increase in the growth rate of R_u than quartz sand. This phenomenon could be attributed to the irregular shape of CSD grains, which produced more rolling and shearing than the quartz sand.

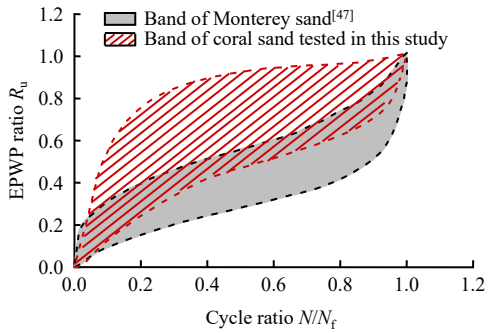


Fig. 16 Generation patterns of EPWP for CSD mixtures

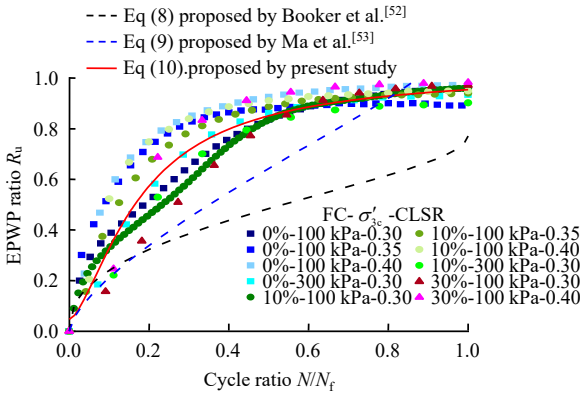
Based on the undrained cyclic triaxial tests of quartz sand, Seed et al.[51] developed an empirical model, and Booker et al.[52] subsequently derived a simplified formulation in Equation (8):

$$R_u = \frac{2}{\pi}\arcsin\left(\frac{N}{N_f}\right)^{\frac{1}{2\theta}} \tag{8}$$

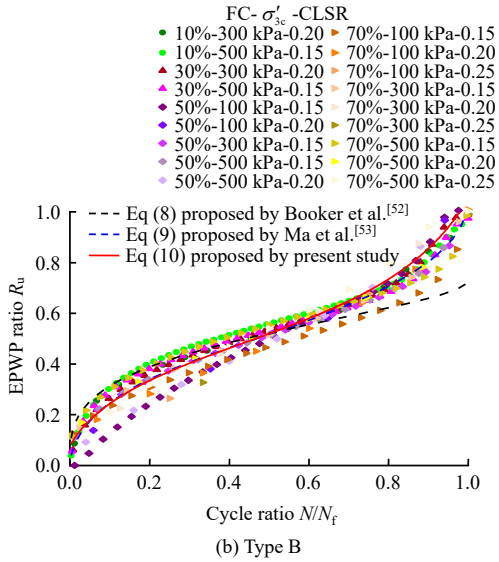
where θ represented an experimentally constant related to the sand type. The results of the R_u of the CSD mixture based on Equation (8) (the black dashed line in Fig.17) indicated that the Booker model did not apply to the R_u prediction of CSD mixtures. Ma et al.[53] proposed a modified Seed model based on the EPWP development characteristics of CSD under undrained cyclic triaxial test conditions, as shown in Equation (9):

$$R_u = a + \frac{2}{\pi}\arcsin\left(\frac{N}{N_f}\right)^{\frac{1}{2\theta}} + b\arctan\left(\frac{N}{N_f}\right) \tag{9}$$

where a and b represented the fitting parameters. As shown by the blue dotted line in Fig.17, although the modified Seed model (Equation (9)) could describe the characteristics of the B-type curve relatively well, its prediction effect on the A-type curve was still unsatisfactory.



(a) Type A



(b) Type B

Fig.17 Comparison of prediction outcomes from EPWP models

Therefore, it was not appropriate to directly apply the existing EPWP models to describe the EPWP development of CSD mixtures. According to the curve characteristics and applicability analysis of EPWP, it was found that the triangular function could better fit the S-shaped curve, and the logarithmic and power functions could better fit the curve with a decreasing slope[54]. Based on this idea, we proposed a new unified EPWP model for CSD mixtures that could characterize both Type A and Type B development patterns, significantly improved prediction accuracy, and the specific formula was shown in Equation (10) as follows:

$$R_{\mathrm{u}} = a + \frac{b}{\pi}\tan\left[\beta\left(\frac{N}{N_{\mathrm{f}}}\right)^{\frac{1}{\theta}} - c\right] \quad (10)$$

where c and β were empirical parameters. Their magnitudes determined the morphology of the vibrating EPWP growth, mainly related to factors such as effective confining pressure, CLSR, and FC, whose specific values were listed in Table 3. The new EPWP model showed a good predictive effect, as illustrated by the red solid line in Fig.17 for both Type A and Type B curves.

Table 3 Fitting parameters for the novel pore water pressure model

Type of curve	Reference	a	b	β	θ	c	R^2
Type A	Booker et al.[52]	—	—	—	0.859	—	−1.96
	Ma et al.[53]	1.210	0.275 0	—	0.622	—	0.55
	This study	1.010	0.034 5	0.653	1.545	1.535	0.92
Type B	Booker et al.[52]	—	—	—	0.400	—	0.67
	Ma et al.[53]	1.896	−0.664 0	—	0.588	—	0.96
	This study	0.463	0.286 0	2.323	0.858	0.941	0.96

5 Conclusions

Undrained cyclic triaxial tests were conducted on saturated CSD mixtures with extensive FC ranges under varying confining pressures and CLSR. Experimental results and corresponding discussions clarified the influence mechanism of FC on the liquefaction resistance, deformation, particle breakage, plastic work and EPWP development of CSD mixtures. The primary findings of this study were as follows:

(1) It was suitable to divide CSD mixtures into two different types, i.e., coarse-grained CSD and fine-grained CSD, and the failure modes of those two were significantly different, and fine-grained CSD was more prone to liquefaction. It provided an important basis for the classification of engineering seismic sites in CSD areas and the implementation of differentiated anti-liquefaction measures.

(2) The liquefaction strength of the coarse-grained CSD decreased as confining pressure increased, whereas that of the fine-grained CSD increased as confining pressure increased. The liquefaction resistance of CRR_{20} of CSD mixtures first decreased before subsequently increasing with increasing FC and reached a minimum value when FC was near the FC_{th}. Consequently, it was recommended that the use of fill materials with an FC close to the FC_{th} be strictly avoided in engineering practice. Furthermore, poorly-graded soil foundations should undergo gradation improvement or dynamic compaction to enhance their stability. When the FC and confining pressure were small (for example, FC=0%-10%, σ'_{3c} = 100 kPa), the deformation of the sample gradually accumulated as the cyclic number N increased. As FC and confining pressure increased, the deformation transformed from a gradual accumulation mode to a slow-rapid development mode.

(3) As FC increased, the particle breakage of the specimens decreased significantly. Nevertheless, an increasing trend in particle breakage was observed at higher confining pressures and CLSR. In addition, the plastic work of CSD mixtures initially decreased before increasing as FC increased, reaching its minimum value when FC was around FC_{th}. This understanding could be practically applied to optimizing CSD compositions for construction and infrastructure projects to enhance durability and performance under varying load conditions.

(4) When FC=0%-10% under a confining pressure of 100 kPa, EPWP development displayed Type A growth, and it progressively shifted to Type B growth with FC and confining pressure increasing. Coarse-grained and fine-grained CSD had different EPWP responses in the third stage of the Type B development pattern, and the EPWP growth rate of coarse-grained CSD gradually slowed down, while it continued to increase for fine-grained CSD. The EPWP development mode of CSD mixtures presented notable differences from that of quartz sand, and a novel development model was established to properly predict the EPWP and R_{u} for both Type A and Type B patterns.

Declaration of competing interest

The authors declare that they have no conflict of interest.

References

[1] CHEN H Y, WANG R, LI J G, et al. Grain shape analysis of calcareous soil[J]. Rock and Soil Mechanics, 2005, 26(9): 1389-1392.

[2] QIAN K, WANG X Z, CHEN J W, et al. Experimental study on permeability of calcareous sand for islands in the South China Sea[J]. Rock and Soil Mechanics, 2017, 38(6): 1557-1564.

[3] ZHU C Q, CHEN H Y, MENG Q S, et al. Microscopic

characterization of intra-pore structures of calcareous sands[J]. Rock and Soil Mechanics, 2014, 35(7): 1831-1836.

[4] HALL E B, GORDON B B. Triaxial testing with large-scale pressure equipment[J]. Laboratory Shear Testing of Soils, 1963, 361: 315-328.

[5] ZHANG J M, ZHANG L, JIANG G S, et al. Research on particle crushing of calcareous sands under triaxial shear[J]. Rock and Soil Mechanics, 2008, 29(10): 2789-2793.

[6] WEI H Z, ZHAO T, HE J Q, et al. Evolution of particle breakage for calcareous sands during ring shear tests[J]. International Journal of Geomechanics, 2018, 18(2): 04017153.

[7] WANG G, ZHA J J, WEI X. Evolution of particle crushing of carbonate sands under cyclic triaxial stress path[J]. Chinese Journal of Geotechnical Engineering, 2019, 41(4): 755-760.

[8] VAHDANI S, PYKE R, SIRIPRUSANEN U. Liquefaction of calcareous sands and lateral spreading experienced in Guam as a result of the 1993 Guam earthquake[C]//Proceedings of 5th US-Japan Workshop on Earthquake Resistant Design of Lifeline Facilities and Countermeasures against Soil Liquefaction. Buffalo, NY, USA: National Center for Earthquake Engineering Research, 1994: 117-134.

[9] CHOCK G, ROBERTSON I, NICHOLSON P, et al. Compilation of observations of the October 15, 2006 Kiholo Bay (Mw 6.7) and Mahukona (Mw 6.0) earthquakes[C]//Proceedings of Earthquake Engineering Research Institute (EERI). Oakland, CA, USA: Earthquake Engineering Research Institute, 2006.

[10] OLSON S M, GREEN R A, LASLEY S, et al. Documenting liquefaction and lateral spreading triggered by the 12 January 2010 Haiti earthquake[J]. Earthquake Spectra, 2011, 27(Suppl.1): 93-116.

[11] D'APPOLONIA D J, D'APPOLONIA E D, BRISSETTE R F. Settlement of spread footings on sand[J]. Journal of the Soil Mechanics and Foundations Division, 1968, 94(3): 735-762.

[12] INDRARATNA B, TENNAKOON N, NIMBALKAR S, et al. Behaviour of clay-fouled ballast under drained triaxial testing[J]. Géotechnique, 2013, 63(5): 410-419.

[13] LADE P V, YAMAMURO J A. Effects of nonplastic fines on static liquefaction of sands[J]. Canadian Geotechnical Journal, 1997, 34(6): 918-928.

[14] POLITO C P, MARTIN J R. Effects of nonplastic fines on the liquefaction resistance of sands[J]. Journal of Geotechnical and Geoenvironmental Engineering, 2001, 127(5): 408-415.

[15] SITHARAM T G, DASH H K, JAKKA R S. Postliquefaction undrained shear behavior of sand-silt mixtures at constant void ratio[J]. International Journal of Geomechanics, 2013, 13(4): 421-429.

[16] DEZFULIAN H. Effects of silt content on dynamic properties of sandy soils[C]//Proceedings of the 8th World Conference on Earthquake Engineering. [S. l.]: [s. n.], 1984: 63-70.

[17] SHEN C K. The effect of fines on liquefaction of sands[C]//Proceedings of the 9th International Conference on Soil Mechanics and Foundation Engineering. [S. l.]: [s. n.], 1977: 381-385.

[18] THRONCOSO J H, VERDUGO R. Silt content and dynamic behavior of tailing sands[C]//Proceedings of the 11th International Conference on Soil Mechanics and Foundation Engineering. [S. l.]: [s. n.], 1985: 1311-1314.

[19] FINN W D L, LEDBETTER R H, WU G X. Liquefaction in silty soils: design and analysis[C]//Ground Failures under Seismic Conditions. [S. l.]: [s. n.], 1994: 51-76.

[20] VAID Y P. Liquefaction of silty soils[C]//Proceedings of Ground Failures Under Seismic Conditions. [S. l.]: [s. n.], 1994: 1-16.

[21] CAO Y L, LAW K T. Energy approach for liquefaction of sandy and clay silts[C]//Proceedings of the 2nd International Conference on Recent Advances in Geotechnical Earthquake Engineering and Soil Dynamics. Rolla, MO, USA: Missouri University of Science and Technology, 1991: 491-497.

[22] LAW K T, LING Y H. Liquefaction of granular soils with non-cohesive and cohesive fines[C]//Proceedings of the 10th World Conference on Earthquake Engineering. [S. l.]: [s. n.], 1992: 1491-1496.

[23] KOESTER J P. The influence of fines type and content on cyclic strength[C].//Ground Failures under Seismic Conditions. [S. l.]: [s. n.], 1994: 17-33.

[24] SINGH S. Liquefaction characteristics of silts[J]. Geotechnical and Geological Engineering, 1996, 14: 1-19.

[25] CHIEN L K, OH Y N, CHANG C H. Effects of fines content on liquefaction strength and dynamic settlement of reclaimed soil[J]. Canadian Geotechnical Journal, 2002, 39(1): 254-265.

[26] VAHIDI-NIA F, BAYESTEH H, KHODAPARAST M. Effect of initial packing density, stress level and particle size ratio on the behavior of binary granular material: a micromechanical approach[J]. Granular Matter, 2020, 22(3): 68.

[27] YANG S L, LACASSE S, SANDVEN R. Determination of the transitional fines content of mixtures of sand and non-plastic fines[J]. Geotechnical Testing Journal, 2006, 29(2): 102-107.

[28] DASH H K, SITHARAM T G. Undrained monotonic response of sand-silt mixtures: effect of nonplastic fines[J]. Geotechnical and Geological Engineering, 2011, 29(1): 47-58.

[29] BELKHATIR M, ARAB A, DELLA N, et al. Experimental study of undrained shear strength of silty sand: effect of fines and gradation[J]. Geotechnical and Geological Engineering, 2012, 30(5): 1103-1118.

[30] HU M J, CUI X, WANG X Z, et al. Experimental study of the effect of fine particles on permeability of the

calcareous sand[J]. Rock and Soil Mechanics, 2019, 40(8): 2925-2930.

[31] ZHANG C Y, CHEN M, HU M J, et al. Effect of fine particles content on shear strength of calcareous sand[J]. Rock and Soil Mechanics, 2019, 40(Suppl.1): 195-202.

[32] SHEN Y, ZHU Y H, LIU H L, et al. Macro-meso effects of gradation and particle morphology on the compressibility characteristics of calcareous sand[J]. Bulletin of Engineering Geology and the Environment, 2018, 77: 1047-1055.

[33] LI T, ZHAO H Y, WEN B H, et al. Experimental study on effects of shape and content of fine particles on strength of calcareous mixed sand[J]. Chinese Journal of Geotechnical Engineering, 2023, 45(7): 1517-1525.

[34] WU Q, YANG Z T, LIU K, et al. Experimental study on influences of fines content on dynamic deformation characteristics of saturated coral sand[J]. Chinese Journal of Geotechnical Engineering, 2022, 44(8): 1386-1396.

[35] WU Y, CUI J, LI C, et al. Experimental study on dynamic characteristics of calcareous sand-gravel mixtures from islands in the South China Sea[J]. Chinese Journal of Rock Mechanics and Engineering, 2022, 41(1): 205-216.

[36] CHEN P S, LU W Q, LIANG X C, et al. Experimental study on liquefaction resistance characteristics of fine-grained coralline soils[J]. Rock and Soil Mechanics, 2023, 44(2): 337-344.

[37] THEVANAYAGAM S, MARTIN G R. Liquefaction in silty soils—screening and remediation issues[J]. Soil Dynamics and Earthquake Engineering, 2002, 22(9): 1035-1042.

[38] THEVANAYAGAM S, SHENTHAN T, MOHAN S, et al. Undrained fragility of clean sands，silty sands，and sandy silts[J]. Journal of the Geotechnical and Geo-environmental Engineering, 2002, 128(10): 849-859.

[39] CHANG W J, CHANG C W, ZENG J K. Liquefaction characteristics of gap-graded gravelly soils in K_0 condition[J]. Soil Dynamics and Earthquake Engineering, 2014, 56: 74-85.

[40] LADE P V, LIGGIO C D, YAMAMURO J A. Effects of non-plastic fines on minimum and maximum void ratios of sand[J]. Geotechnical Testing Journal, 1998, 21: 336-347.

[41] Ministry of Water Resources of the People's Republic of China. GB/T 50123 — 2019 Standard for soil test method[S]. Beijing: China Planning Press, 2019.

[42] ZUO L, BAUDET B A. Determination of the transitional fines content of sand-non-plastic fines mixtures[J]. Soils and Foundations, 2015, 55(1): 213-219.

[43] WU Q, CHEN G X, ZHOU Z L, et al. Influences of fines content on cyclic resistance ratio of fines-sand-gravel mixtures[J]. Chinese Journal of Geotechnical Engineering, 2017, 39(6): 1038-1047.

[44] ZHANG K X. Liquefaction stress conditions of saturated sand[J]. Earthquake Engineering and Engineering Vibration, 1984, 4(1): 99-109.

[45] MARTIN G R, SEED H B, FINN W D L. Fundamentals of liquefaction under cyclic loading[J]. Journal of the Geotechnical Engineering Division, 1975, 101(5): 423-438.

[46] KARIM M E, ALAM M J. Effect of non-plastic silt content on the liquefaction behavior of sand-silt mixture[J]. Soil Dynamics and Earthquake Engi- neering, 2014, 65: 142-150.

[47] HARDIN B O. Crushing of soil particles[J]. Journal of Geotechnical Engineering, 1985, 111(10): 1177-1192.

[48] ATHURSON J H. The introduction to the mechanics of soils & foundations: through critical state soil mechanics[M]. London: McGraw Hill, 1993.

[49] ZHANG J M, XIE D Y. A practical algorithm for calculating the increase of pore water pressure in saturated sand under vibration[J]. Journal of Hydraulic Engineering, 1991, 22(8): 45-51.

[50] LEE K L, ALBAISA A. Earthquake induced settlements in saturated sands[J]. Journal of the Geotechnical Engineering Division, 1974, 100(4): 387-406.

[51] SEED H B, MARTIN P P, LYSMER J. Pore-water pressure changes during soil liquefaction[J]. Journal of the Geotechnical Engineering Division, 1976, 102(4): 323-346.

[52] BOOKER J R, RAHMAN M S, SEED H B. GADFLEA—a computer program for the analysis of pore pressure generation and dissipation during cyclic or earthquake loading[R]. Berkeley: Earthquake Engineering Research Center, University of California, 1976.

[53] MA W J, CHEN G X, LI L. Experimental study on liquefaction characteristics of saturated coral sand in Nansha Island under cyclic loading[J]. Chinese Journal of Geotechnical Engineering, 2019, 41(5): 981-988.

[54] LIU Han-long, ZHANG Yu, GUO Wei, et al. A prediction model of dynamic pore water pressure for MICP-treated calcareous sand[J]. Chinese Journal of Rock Mechanics and Engineering, 2021, 40(4): 790-801.